Thermal Science and Engineering Progress 59 (2025) 103343

Contents lists available at ScienceDirect

Thermal Science and Engineering Progress

journal homepage: www.sciencedirect.com/journal/thermal-science-and-engineering-progress

Enhancing LHTES efficiency using asymmetric hexagon anisotropic metal foam layer: A comparative study on orientation and scale

Masoud Mozaffari [a,b], Ahmad Hajjar [c], Mikhail Sheremet [d], Obai Younis [e,f], Mohammad Ghalambaz [g,d,*]

[a] Department of Mechanical Engineering, Najafabad Branch, Islamic Azad University, Najafabad 85141-43131 Iran
[b] Artificial Intelligence and Simulations Research Group, SimoAI OU, Tallinn 10117 Estonia
[c] Center for Environmental Intelligence and College of Engineering and Computer Science, VinUniversity, Hanoi, Viet Nam
[d] Laboratory on Convective Heat and Mass Transfer, Tomsk State University 634050 Tomsk, Russia
[e] Department of Mechanical Engineering, College of Engineering in Wadi Alddwasir, Prince Sattam Bin Abdulaziz University, Saudi Arabia
[f] Department of Mechanical Engineering, Faculty of Engineering, University of Khartoum, Sudan (the)
[g] Department of Mathematics, Saveetha School of Engineering, SIMATS, Chennai, India

ARTICLE INFO

Keywords:
Asymmetric Hexagon Geometry
Anisotropic Metal Foam Layer (AMFL)
Latent Heat Thermal Energy Storage (LHTES)
Copper Metal Foam
Phase Change

ABSTRACT

The latent heat thermal energy storage devices can store a notable amount of energy in a fairly compact space with minimal environmental impact. However, the heat transfer rate in these systems is limited by inherited low thermal conductivity of most organic materials such as paraffins. This research focuses on addressing the impact of using an engineered anisotropic metal foam layer on heat transfer improvement of latent heat thermal energy storage (LHTES) units. The comprehensive two heat equation models, together with a finite element method, were employed to simulate the energy storage in LHTES unit. The study demonstrates that increasing the size of the Anisotropic Metal Foam Layer (AMFL) significantly enhances the melting of paraffin. The orientation of the AMFL also plays a crucial role, with the larger side positioned near the hot wall contributing more effectively to PCM melting. This optimal arrangement led to a reduction in melting duration by up to 5.28%. AMFL reduced the melting time by 8.2% in case d2 compared to a case with uniform metal foam.

1. Introduction

Latent Heat Thermal Energy Storage (LHTES) systems have become increasingly critical in addressing the intermittency and unreliability of renewable energy sources such as solar and wind power. As countries globally advocate for the reduction of carbon footprints and seek energy security through renewable sources, the efficient utilization of these energy systems is paramount. LHTES systems offer a solution by storing excess energy during peak production times and releasing it upon demand, thus enhancing energy availability and grid stability. The inherent property of phase change materials (PCMs) in LHTES systems to absorb and release heat during phase transitions makes them excellent candidates for energy storage. However, the low thermal conductivity of PCMs presents a significant limitation, often resulting in slower thermal response times during the charging and discharging processes [1,2].

Improving the heat transfer within LHTES systems is essential for optimizing energy storage and retrieval efficiencies. Traditional methods have primarily focused on passive techniques such as the integration of fins [3], the modification of system geometry [4], integration of nanoparticles [5,6], and other passive methods [7]. Magnetohydrodynamic effects have also shown promising outcomes in control of flow and heat transfer [8–10].

Recent advancements in enhancing LHTES efficiency have highlighted the significant impact of incorporating metal foams within the PCM. Metal foams, with their high porosity and surface area, enhance the thermal conductivity of the PCM, thereby improving the melting and solidification rates crucial for rapid energy storage and release. The introduction of metal foams into LHTES systems has been shown to significantly reduce the time required for the PCM to reach its phase change temperature, thus enhancing the system’s overall energy storage rate and efficiency [11,12].

---

* Corresponding author.
E-mail addresses: masoodmozafari66@yahoo.com (M. Mozaffari), ahmad.h@vinuni.edu.vn (A. Hajjar), sheremet@math.tsu.ru (M. Sheremet), o.elamin@psau.edu.sa (O. Younis), m.ghalambaz@gmail.com (M. Ghalambaz).

https://doi.org/10.1016/j.tsep.2025.103343
Received 9 November 2024; Received in revised form 30 January 2025; Accepted 31 January 2025

Experimental studies have demonstrated that the incorporation of metal foams can lead to an increase in the effective thermal conductivity of PCMs by up to ten times compared to traditional methods. This increase is primarily due to the metal foam's ability to facilitate greater internal convection and reduce thermal resistance at the solid–liquid interface of the PCM. Moreover, metal foams can be engineered with varying pore sizes and densities, allowing for customization based on specific thermal performance requirements [12,13].

Integrating metal foams into LHTES systems can enhance thermal performance but also adds to the cost and weight. Additionally, metal foams do not contribute to latent heat storage, reducing the overall volumetric energy density. Therefore, strategies that either minimize the use of metal foams or increase the storage rate without adding more foam could significantly improve the feasibility of LHTES units for energy storage applications [14,15]. Several researchers have investigated the impact of metal foams on energy storage aspects of LHTES systems [14,16,17]. The studies using metal foam can be divided in three categories of regular metal foams, metal foams with porosity gradient, and anisotropic metal foams.

Considering regular metal foams, several recent studies have investigated LHTES systems. The integration of metal foams into LHTES systems significantly enhances energy storage and heat transfer efficiency. These systems, typically hampered by the insufficient PCMs' heat conductivity, benefit from the high thermal conductivity and porous structure of metal foams. This review compiles several studies to assess the effects of regular metal foams on the energy storage and heat transfer performance of LHTES units, examining both fully and partially filled configurations. A primary focus in this field is optimizing metal foam characteristics such as porosity and pores per inch (PPI), crucial for improving heat transfer rates. Research indicates that metal foams with a porosity of 0.90 can reduce the melting time of the PCM by 1110 s compared to those with a porosity of 0.99, underscoring porosity's vital role in thermal performance [18]. Additionally, using lower PPI foams, such as 10 PPI, can decrease the melting time by 1280 s compared to 100 PPI foams, proving that coarser foams are more effective in these systems [18].

In partially filled LHTES units, the placement of metal foam is key to the overall thermal behavior of the system. Studies have shown that strategically positioned metal foams, even in diagonal configurations, can significantly minimize melting time without substantially sacrificing energy storage capacity. For example, a numerical investigation demonstrated that adjusting the foam's porosity to 0.88 almost matched the energy storage performance of pure PCM, with only a 4 % difference, suggesting that partial filling with strategically placed foams can optimize the balance between heat transfer and energy storage [19]. Further investigations highlight the impact of metal foam on enhancing thermal behavior more significantly than nanoparticles alone. It was observed that the height ratio of metal foam filling did not drastically affect the heater temperature, indicating that the presence and configuration of the foam are more critical than its filling extent [20].

Experimental studies integrating metal foams with other systems like thermoelectric generators have shown that a combination of metal foam/PCM can lower heat-source temperatures by 33.5 °C compared to systems using metal foam alone. However, this thermal management improvement may come at the expense of reduced power generation, highlighting necessary trade-offs in dual-purpose systems [21]. The filling height of metal foam also influences LHTES performance. Research on thermal storage tanks identified an optimal filling ratio that maximized energy efficiency and reduced the full melting time by 15.7 % while conserving 5 % of foam mass. Notably, high-porosity foams showed minimal sensitivity to filling ratio changes, whereas lower porosity foams benefited more from optimized ratios [22]. This supports the concept that partial filling can enhance energy storage while minimizing material costs. The design and geometry of LHTES units significantly affect the performance of systems enhanced with metal foams. Studies have found that higher inclination angles and specific designs, like vertical shell and convergent tube systems, can lead to faster energy storage. Additionally, innovative designs such as bottom-cut in LHTES units filled with metal foam showed that a cross-cut ratio of 0.6 could increase the heat storage rate by 18.84 % and enhance natural convection significantly, optimizing the melting performance [23]. Exploring layered configurations, a study revealed that an LHTES unit with a top layer of high porosity foam reduced charging time by 32 % to 837 s. This indicates that using various metal foam configurations within a single unit could be a promising strategy for enhancing energy storage performance while maintaining a low material weight [24].

Incorporating metal foams with variable porosity into LHTES systems has markedly improved their efficiency. These foams, designed with porosity gradients, effectively address the low thermal conductivity and uneven heat distribution challenges associated with PCMs due to natural convection. Research highlights significant enhancements in LHTES units utilizing non-uniform porosity metal foams. For instance, a numerical analysis of a shell-and-tube thermal energy storage system revealed that a porosity gradient increased along the y-direction, which boosted the melting rate and the average heat transfer rate by 21.6 % over a uniform porosity of $\varepsilon = 0.94$. Specifically, a gradient of $\varepsilon = 0.94 + 0.267y$ during melting significantly improved heat transfer effectiveness [25]. Additionally, when the gradient increased along the outer radius, the efficiency of heat exchange adjacent to the heating wall enhanced, albeit at the expense of a slower phase change process near the outer wall, with the most effective heat transfer rate occurring at $\varepsilon = 0.88 + 0.6r$ [25].

Optimization techniques for two-dimensional porosity gradients also yielded positive outcomes. Using superposition and 2D iterative methods to adjust the interaction between horizontal and vertical gradients led to an 11.32 % decrease in full melting time for the optimally adjusted system, which improved temperature uniformity and enhanced natural convection [26]. Another study introduced a novel metal foam design with horizontally and vertically varying porosity. This design, utilizing functionally graded metal foam, increased convection intensity during the melting stages. Both horizontal and vertical gradients not only reduced the overall melting time but also boosted the average power density by 15.8 % compared to systems with uniform porosity. This gradient combination effectively balanced the uneven melting inherent to natural convection [27].

The exploration of anisotropic (heterogeneous) metal foams in LHTES units offers transformative benefits for energy storage and heat transfer optimization. Anisotropic metal foams can be fully or partially filled within LHTES units, greatly enhancing their performance by addressing the uniformity issues inherent in traditional foams. Anisotropic porous skeletons have demonstrated exceptional thermal management capabilities, such as reducing chip surface temperatures significantly more effectively than traditional aluminum heat sinks. These skeletons, prepared using the ice-template method, not only facilitate more effective PCM adsorption, achieving a pore utilization rate of 98.22 %, but also enhance the heat transfer predominantly in the axial direction, as confirmed by numerical models using the Lattice-Boltzmann method. This setup improves the average heat storage density and supports superior heat transfer mechanics by reducing tortuosity in the melting process of PCMs, showing a heat storage density of 94.17 J/g [28].

In tilted enclosure scenarios, anisotropic metal foams with engineered local properties significantly impact the characteristics of phase change and the time required for charging in LHTES units. Mathematical modeling depicted that an optimum tilt angle, coupled with an anisotropic angle, maximizes charging power, reducing charging time by up to 20 % compared to regular foams, without sacrificing capacity or increasing weight [29]. Further mathematical modeling of heterogeneous metal foams highlighted that controlled heterogeneity in metal foams could alter melting times significantly. Up to 24 %, the heterogeneity angle can boost the heat transfer rate and reduce the thermal charging time depending on its angle, offering a substantial

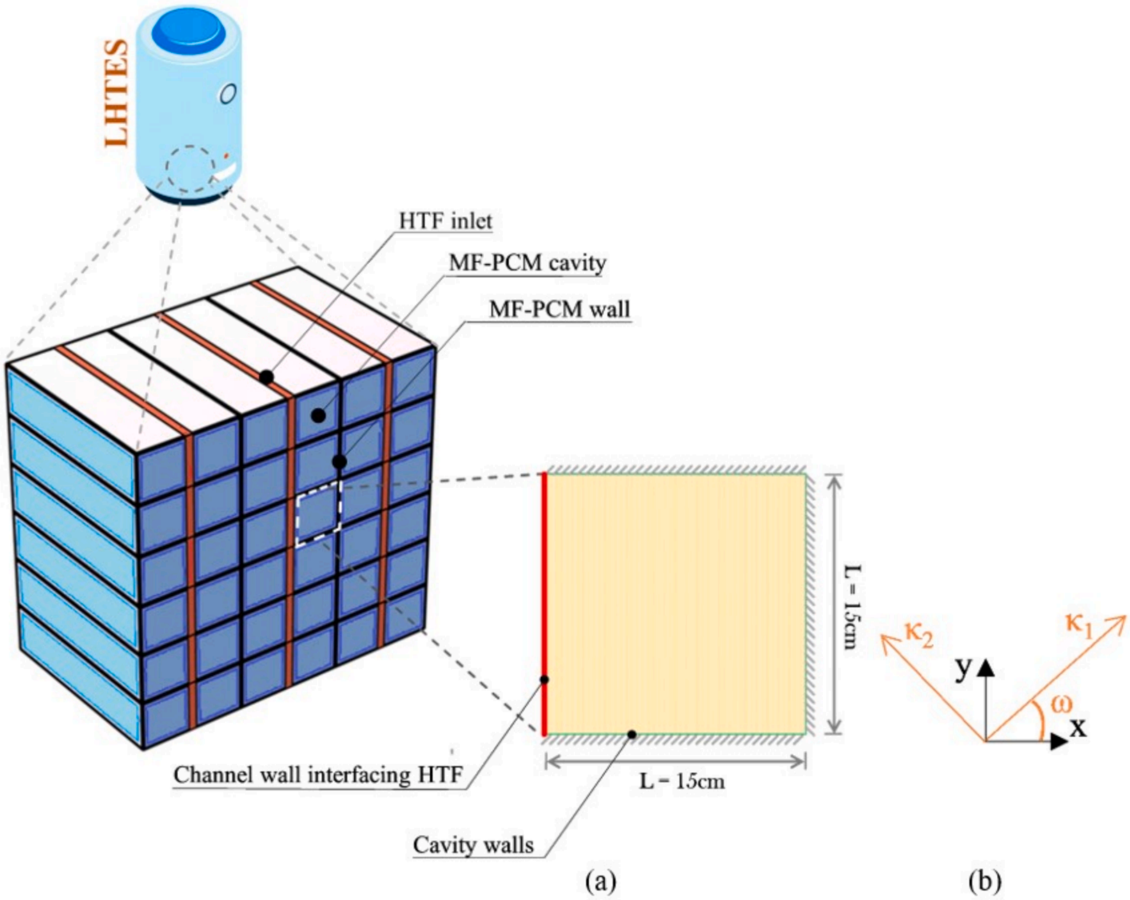

Fig. 1. Overview of a multi-channel LHTES unit, depicting the heat transfer fluid (HTF) inlet and a detailed 2D cross-section of a single storage compartment in the system. The PCM units are the duct shape enclosures where HTF flows in the space between the PCM units. The LHTES contains a series of PCM channels. (a) Illustration of the storage area; (b) Explanation of the alignment concerning anisotropic angles (ω).

improvement over conventional metal foams [30]. Exploring dual-layer metal foam configurations using a neural network design approach, it was found that adjusting porosity and the anisotropic angle can reduce melting times dramatically. A slight increase in porosity, for instance, was shown to decrease melting time by 66 %. This approach integrates advanced analytics to optimize phase change heat transfer, pinpointing that an anisotropic angle of 0° and a specific porosity range provides the most efficient heat transfer [31].

Utilizing ice templated honeycomb-like porous copper foam further underscores the potential of anisotropic foams. These structures, filled with phase change composites, achieve significantly higher axial and lateral thermal conductivities due to their directional channels, offering improved thermal transfer properties for diverse applications [32]. Incorporation of woven metal fibers with anisotropic features into PCMs also marks a significant advancement. Studies using three-dimensional lattice Boltzmann modeling reveal that these fibers enhance heat transfer rates more effectively than traditional straight fibers, especially at higher porosities. By adjusting the anisotropic degree of these fibers, the energy storage rate can be accelerated by 40 %, showcasing the profound impact of anisotropic configurations in optimizing the thermal performance of LHTES units [33].

The literature review indicates that anisotropic metal foams can improve heat transfer rates by locally impacting the porous structure and the direction of heat transfer. The effects of anisotropic strength and angle on the melting of PCMs and the energy storage rate in LHTES units have been explored. However, the impact of combining regular and anisotropic metal foam layers on the characteristics of LHTES units has not yet been investigated. Therefore, this research study seeks to examine the effect of using an asymmetric hexagonal anisotropic metal foam layer on the energy storage characteristics of LHTES units for the first time.

2. Physical problem

The research work provides a comprehensive analysis of an LHTES system, as visualized in Fig. 1, featuring an elaborate network of water channels that facilitate heat distribution. Within this setup, water act as a heat transfer medium, circulating through channels to efficiently deliver heat to the paraffin wax PCM encased in copper metal foam. The PCM, exposed to a temperature (T_h) above its melting point (T_{fu}), transitions from solid to liquid, capturing thermal energy effectively. This system configuration is designed to capture and store surplus heat, enhancing the system's capabilities in energy conservation and management. The LHTES unit is enclosed in a sealed 15 cm by 15 cm compartment, where heat is applied from the left side and the remaining boundaries are insulated to prevent heat exchange. Further details in Fig. 2 depict varied cavity designs within the LHTES, featuring both uniform and anisotropic metal foam layer (AMFL), with a particular focus on the asymmetrical hexagon AMFL. This layer is strategically engineered to maximize heat absorption from the heated boundary and disperse it through the PCM, away from the direct heat source. The configurations vary in the placement and size of the AMFL to evaluate their influence on the system's thermal efficiency and to identify the most effective layout for enhancing the PCM's melting process through diverse orientations and sizes inside the MF structure. The AMFL occupies varying proportions of the total MF area across four distinct

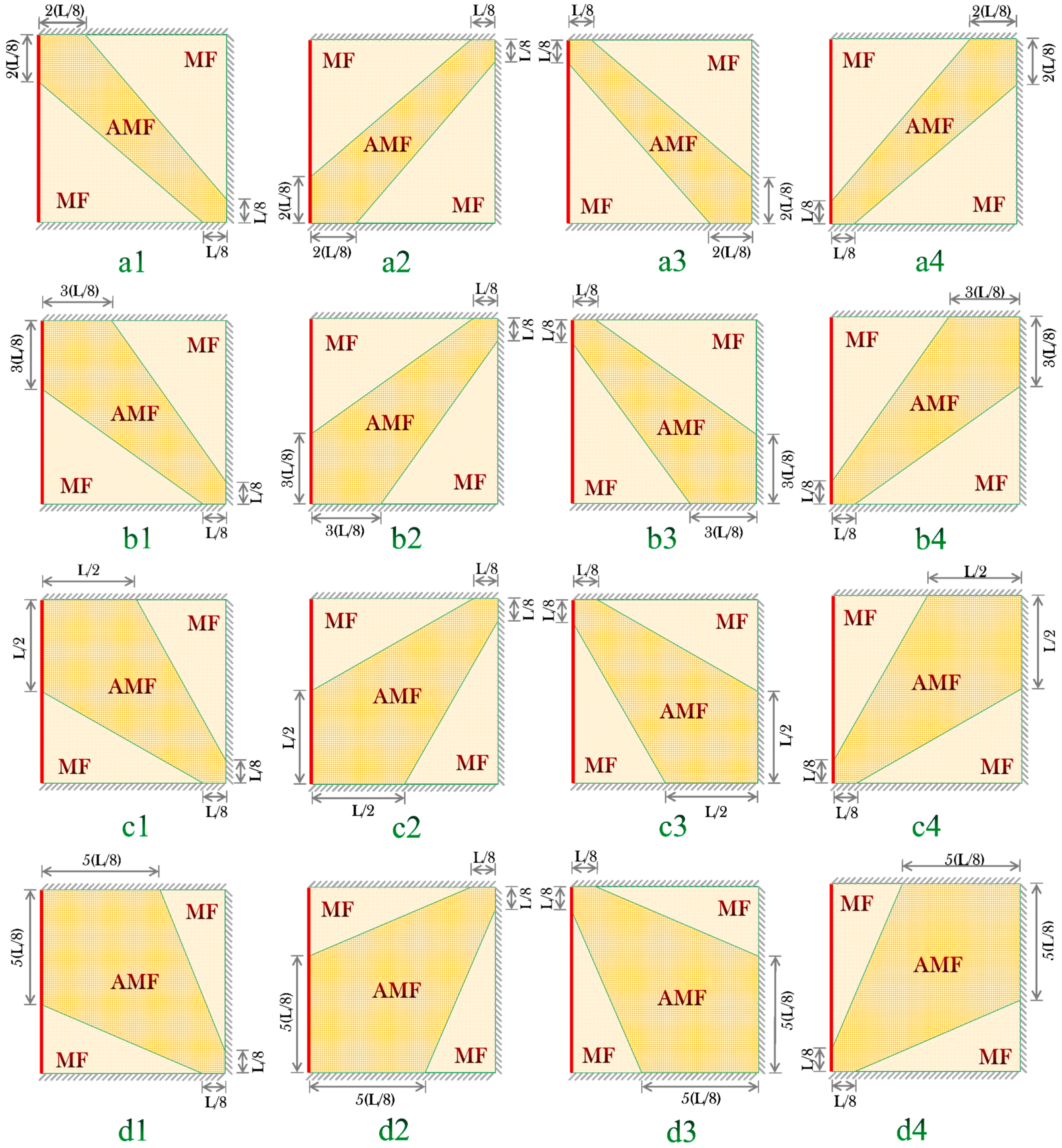

Fig. 2. Anisotropic metal foam (AMF) layer in asymmetrical hexagon shapes, with Group a covering 34.3%, Group b covering 45.3%, Group c covering 56.3%, and Group d 67.2% of the total MF area across various configurations. The remaining areas are filled with uniform MF.

groups, each containing four configurations:

- **Group a (a1 to a4):** incorporates designs with the smallest proportion of AMFL, encompassing 34.3 % of the total MF area. This group assesses the minimal extent of AMFL necessary for effective heat transfer and PCM melting efficiency.
- **Group b (b1 to b4):** demonstrates a moderated increase in AMFL coverage, occupying 45.3 % of the total MF area. These setups are designed to examine the incremental effects on thermal conductivity as AMFL coverage expands.
- **Group c (c1 to c4):** displays a significant proportion of AMFL, comprising 56.3 % of the total MF area. This series is aimed at determining the optimal coverage ratio for maximizing thermal efficiency while maintaining system stability.
- **Group d (d1 to d4):** utilizes the most extensive AMFL coverage, filling 67.2 % of the total MF area. These configurations test the upper limits of AMFL utilization in enhancing heat distribution

across the PCM, investigating the impacts of substantial AMFL deployment.

Each configuration is analyzed to optimize the AMFL's placement, refining melting efficiency and thermal conductivity of the PCM. Controlled by an anisotropy parameter (*Kn*) and an angle (ω), set at 0.3 and 0° respectively, the designed directional attributes of the AMFL provide a perpendicular orientation relative to the heat source, influencing both heat conduction and permeability. This setup is key in determining how variations in the AMFL's structure and orientation impact the thermal properties of the unit.

The comprehensive analysis includes documenting the effectiveness of each configuration in improving heat absorption and distribution within the LHTES unit, focusing on achieving optimal thermal pathways and melting times. This investigation not only provides great insights into the geometric manipulation of the AMFL but also demonstrates major improvement in energy storage efficiency and retrieval capabilities inside the system.

3. Principal equations

This research encompasses a detailed examination of three interrelated sectors in the study domain: the boundary of the copper conduit, the homogeneous metal foam-PCM (MF-PCM) composite, and the anisotropic MF-PCM composite. The incorporation of the Boussinesq hypothesis addresses the interactions between temperature variations and density changes in the system. The study assumes a zero-slip velocity condition at the boundary wall, operating under the assumption that the PCM behaves as a two-dimensional uniform flow regime in an incompressible Newtonian fluid. While the Energy equation provides insights into the PCM's heat uptake during the phase transition and temperature spread throughout the MF, the Continuity equation ensures the conservation of mass during the PCM's liquefaction, working with the Momentum equation to map the movement of the liquefied PCM, acknowledging both viscosity-related and environmental factors. The core principles of conservation of mass, momentum, and energy are encapsulated by partial differential equations (PDEs), tackled using finite element method (FEM). This method adeptly handles the complexities arising from nonlinear dynamics during phase changes. Collectively, termed as Equation (1), these equations proficiently simulate the melting process of PCM and its distribution through the MF [34–36].

$$\begin{cases} \dfrac{\partial u_i}{\partial x_i}=0 \\ \dfrac{\partial u_i}{\partial t}+\dfrac{1}{\varepsilon}\left(u_j\dfrac{\partial u_i}{\partial x_j}\right)U=-\dfrac{\varepsilon}{\rho}\left(\dfrac{\partial p}{\partial x_i}\right)+\dfrac{\mu}{\rho}\left(\dfrac{\partial u_i}{\partial x_i\partial x_j}\right)+F_i \\ \rho C_p\dfrac{\partial T_i}{\partial t}=k\left(\dfrac{\partial T_i}{\partial x_i\partial x_j}\right)+q_{gen} \end{cases} \qquad (1)$$

The flow dynamics in the MF are modeled using the Darcy-Brinkman-Forchheimer framework, offering a robust formulaic foundation for studying fluid movement through porous media. The energy conservation equation incorporates the local thermal non-equilibrium approach to independently handle thermal transmission in all stages of the metal foam and phase change material. This approach separates the domains of wax phase change material and copper metal foam with a detailed array of formulas, which are specifically adapted by modifying permeability and porosity parameters to suit each domain to accommodate the exchange of energy between the different phases, coupling source terms are introduced. In scenarios where the PCM is molten, either uniformly or in anisotropic formations, the phenomenon of natural conservation is tackled using both continuity and momentum equations. The phase transitions are simulated using the enthalpy-porosity technique, which equates the partially fluid state in the mushy region with the flow dynamics in porous structures. Including specific source terms in the momentum equations, this simulation addresses the immobilization of unmelted PCM, determined by the melt fraction (ϕ). It also integrates an additional term that accounts for the opposition introduced by both the porous structure and the phase transition, adjusting the fluid's momentum according to the liquid fraction $\phi(T)$ in the mushy region. This nuanced approach provides a sophisticated depiction of the fluid dynamics influenced by phase changes inside the MF in the horizontal direction as follows [34–36]:

$$\frac{1}{\varepsilon}\rho_{PCM}\left(\frac{\partial u}{\partial t}\right)+\frac{1}{\varepsilon^2}\rho_{PCM}\left(u\frac{\partial u}{\partial x}+v\frac{\partial u}{\partial y}\right)=-\left(\frac{\partial p}{\partial x}\right)+\frac{1}{\varepsilon}\mu_{PCM}\left(\frac{\partial u^{2}}{\partial x^2}+\frac{\partial u^{2}}{\partial y^2}\right)$$
$$-u\left(\frac{\mu_{PCM}}{\kappa}\right)-u\left(\rho_{PCM}\frac{C_F}{\sqrt{\kappa}}|U|\right)+u\left(A_{mush}\frac{(1-\phi(T))^2}{\gamma_{mush}+\phi^3(T)}\right) \qquad (2)$$

The terms "*MF*", "*PCM*", and "*eff*" are shorthand for copper metal foam, paraffin-based phase change material, and their respective effective properties. The equation governing momentum in the y-direction incorporates the same fundamental components with an added term for convection heat transfer, emphasizing the role of buoyancy in influencing flows in the molten PCM. This y-directional momentum equation is formulated as follows:

$$\frac{1}{\varepsilon}\rho_{PCM}\left(\frac{\partial v}{\partial t}\right)+\frac{1}{\varepsilon^2}\rho_{PCM}\left(u\frac{\partial v}{\partial x}+v\frac{\partial v}{\partial y}\right)=-\left(\frac{\partial p}{\partial y}\right)+\frac{1}{\varepsilon}\mu_{PCM}\left(\frac{\partial v^{2}}{\partial x^2}+\frac{\partial v^{2}}{\partial y^2}\right)$$
$$-v\left(\frac{\mu_{PCM}}{\kappa}\right)-v\left(\rho_{PCM}\frac{C_F}{\sqrt{\kappa}}|U|\right)+v\left(A_{mush}\frac{(1-\phi(T))^2}{\gamma_{mush}+\phi^3(T)}\right)+g\rho_{PCM}\beta_{PCM}(T-T_0) \qquad (3)$$

In Equation (4) [37], which focuses on the conservation of energy inside the phase change state, the effective thermal conductivities of the PCM ($k_{\mathrm{eff},PCM}$) and the MF ($k_{eff,MF}$) are critical in illustrating how the pore structures affect thermal conductivity, as referenced [37]. This equation highlights the mechanisms of heat transfer, showcasing convective interactions between the PCM and the adjacent copper, as well as diffusion through the PCM itself. It also incorporates terms that account for the thermal energy absorbed during the phase change state.

$$\varepsilon(\rho C_p)_{PCM}\frac{\partial T_{PCM}}{\partial t}+(\rho C_p)_{PCM}\left(u\frac{\partial T_{PCM}}{\partial x}+v\frac{\partial T_{PCM}}{\partial y}\right)=$$
$$k_{eff,PCM}\left(\frac{\partial^2 T}{\partial x^2}+\frac{\partial^2 T}{\partial y^2}\right)+h_v(T_{MF}-T_{PCM})-\varepsilon\rho_{PCM}L_{PCM}\frac{\partial\phi(T)}{\partial t} \qquad (4)$$

The dynamics of PCM within the mushy zone are intricately governed by a set of equations that incorporate various parameters such as porous permeability (κ), the heat of fusion (L), the Forchherimer coefficient (C_F), and the coefficient of thermal expansion (β). These parameters, integral to the formulation, help define the behavior of PCM as it transitions between states

In the simulation of PCM, the application of the Carman-Kozeny equation significantly influences the control over PCM velocities, especially as it pertains to the structure of the melting front. This equation employs the A_{mush} parameter to regulate the flow dynamics, marking a notable shift in flow resistance from a free-following state, indicated by a value of 6×10^6 Pa.s/m^2, to a constrained state inside the MF region, where the value rises sharply to 1×10^{10} Pa.s/m^2. This adjustment is crucial for managing the flow solidified or semi-solid zones. The model's approach to the mushy zone is to conceptualize it as a porous medium, where the transition from liquid to solid dramatically reduces both porosity and permeability. This reduction leads to an almost stagnant fluid velocity, epitomizing the damping effect of body forces in these areas. Additionally, the model integrates a small constant, γ_{mush}, set at 0.001, to avert any potential division by zero, ensuring the model's stable operation. Furthermore, the relationship between the melting volume fraction, ϕ, and temperature is critical, as it delineates how changes in temperature affect the PCM's melting behavior. This interplay is vital for understanding and optimizing the thermal management properties of PCMs in various applications [38]. In the mushy zone, $\phi(T)$ linearly describes how the PCM shifts from solid to liquid across a temperature range defined by T_{fu} and ΔT_{fu}, the fusion temperature and its variance, respectively. Here, the PCM exists in a state where solid and liquid phases intermingle. The viscosity equation, when $\mu = (1-\phi) \times a + \mu_{\mathrm{PCM,l}}\,\phi$, "$a$ " is set to a large number of 10^4 $Pa.s$, adjusts based on the value of ϕ. At $\phi = 1$, the viscosity closely aligns with the liquid PCM's standard dynamic viscosity, $\mu_{PCM,l}$. Conversely, a decrease in ϕ to zero heightens viscosity in the solid portions, thus increasing flow resistance effectively [38].

$$\phi(T) = \begin{cases} 0 & T < T_{\mathrm{fu}} - \dfrac{\Delta T_{\mathrm{fu}}}{2} & (\text{Solid}\,PCM) \\ \dfrac{1}{2} + \dfrac{(T - T_{\mathrm{fu}})}{\Delta T_{\mathrm{fu}}} & T_{\mathrm{fu}} - \dfrac{\Delta T_{\mathrm{fu}}}{2} \le T \le T_{\mathrm{fu}} + \dfrac{\Delta T_{\mathrm{fu}}}{2}\ (\text{Mushy zone}) & \\ 1 & T > T_{\mathrm{fu}} + \dfrac{\Delta T_{\mathrm{fu}}}{2} & (\text{Liquid}\,PCM) \end{cases} \tag{5}$$

In this instance, l denotes the liquid phase and s represents the unmelted phase of the PCM, their thermophysical properties calculated through a linear weight average.

$$\left(\rho C_p\right)_{PCM} = \varphi\left(\rho C_p\right)_{\mathrm{s}} + (1 - \varphi)\left(\rho C_p\right)_{\mathrm{l}} \tag{6a}$$

$$\rho_{PCM} = \varphi\rho_{\mathrm{s}} + (1 - \varphi)\rho_{\mathrm{l}} \tag{6b}$$

In the energy conservation within the MF phase, the formula uses the term $(1\text{-}\varepsilon)(\rho C_p)_{MF}$ to show how the copper foam's effective heat capacity accounts for porosity (ε), illustrating energy conservation, with $\varepsilon = 0.95$ considered in the current simulation:

$$(1 - \varepsilon)\left(\rho C_p\right)_{MF}\frac{\partial T_{MF}}{\partial t} = k_{eff,MF}\left(\frac{\partial^2 T_{MF}}{\partial x^2} + \frac{\partial^2 T_{MF}}{\partial y^2}\right) + h_v(T_{PCM} - T_{MF}) \tag{7}$$

In the development of the asymmetric hexagon AMFL, the design takes into account how permeability and thermal conductivity differ with changing orientations. This adaptation is impacted by the anisotropy angle (ω) and the anisotropic parameter (Kn), with a strategic reinforcement of the ligaments within the MF layer along a designated direction. To achieve the most efficient thermal performance of the LHTES, $Kn = 0.3$ and $\omega = 0^\circ$ are set for all scenarios. Such enhancements increase thermal conductivity while concurrently diminishing permeability. To articulate these variations, the model includes trigonometric functions of ω, which aid in translating these properties from principal to actual directions. The behavior is further defined by a second-order tensor that interlinks the intrinsic properties, k_1 and $k_{2,}$ with the anisotropy angle. This complex relationship is detailed in the equations that follow, providing a comprehensive framework for understanding the anisotropic behavior within the system. [39].

$$\kappa = \begin{bmatrix} \kappa_2(\sin\omega)^2 + \kappa_1(\cos\omega)^2 & (\kappa_1 - \kappa_2)(\cos\omega)(\sin\omega) \\ (\kappa_1 - \kappa_2)(\cos\omega)(\sin\omega) & \kappa_2(\cos\omega)^2 + \kappa_1(\sin\omega)^2 \end{bmatrix} \tag{8a}$$

$$k_{\mathrm{eff},\,MF} = \begin{bmatrix} k_2(\sin\omega)^2 + k_1(\cos\omega)^2 & (k_1 - k_2)(\sin\omega)(\cos\omega) \\ (k_1 - k_2)(\sin\omega)(\cos\omega) & k_2(\cos\omega)^2 + k_1(\sin\omega)^2 \end{bmatrix} \tag{8b}$$

In the study of copper MF, the average thermal conductivity and permeability are symbolized by k_{m} and κ_m, respectively. These values are established using the methods described in references [40–42]. The factor that describes anisotropy within the material is denoted by Kn, with $Kn = 0$ indicating that the MF is isotropic. The formulas for calculating thermal conductivity in copper MF are given by $k_1 = (1 + Kn) \times k_{\mathrm{m}}$ and $k_2 = (1\text{-}Kn) \times k_{\mathrm{m}}$. Correspondingly, permeability is calculated using the equations $\kappa_1 = (1\text{-}Kn) \times \kappa m$, $\kappa_2 = (1 + Kn) \times \kappa_{\mathrm{m}}$. Various sources, specifically references [34,37], mention an equation that is applied to calculate the effective thermal conductivity of the PCM. The noted porosity range indicates that the MF is highly porous. It is also important to consider equations that include the parameters κ_{tor} and d_{fs} to calculate the thermal conductivity of copper MF as outlined in reference [34,37,43]:

$$\frac{1}{\kappa_{tor}} = \frac{\sqrt{9 - 8\varepsilon}}{2\varepsilon}\cos\left\{\frac{4\pi}{3} + \frac{1}{3}\cos^{-1}\left(\frac{8\varepsilon^2 - 36\varepsilon + 27}{\sqrt{(9 - 8\varepsilon)^3}}\right)\right\}d_{fp} + \frac{3}{4\varepsilon} \tag{9}$$

In which the pores per inch (PPI) characteristic and d_{fp} are defined as below, with PPI = 5 considered in the current study for computations:

$$d_{fp} = \frac{0.0254}{PPI} \tag{10}$$

$$\frac{d_{fs}}{d_{fp}} = \left(\frac{59}{50}\right)\left(\frac{1 - \varepsilon}{3\pi}\right)^{\frac{1}{2}}\left(\frac{1}{1 - \exp(25(\varepsilon - 1))}\right) \tag{11}$$

Preserving the structural integrity of the MF necessitates controlling the anisotropic factor effectively. Calculations for the average permeability (κ_{a}) and effective thermal conductivity (k_{a}) of the MF included findings from earlier studies [34,37,43].

$$\kappa_a = \left(\frac{\varepsilon d_{fp}\sqrt{\frac{\kappa_{tor}}{3\varepsilon}}}{6}\right)^2 \frac{1}{(\kappa_{tor} - 1)\kappa_{tor}} \tag{12}$$

The evaluation involved computing the Forchheimer coefficient (C_F) as outlined below [43]:

$$C_F = 0.00212\left(\frac{d_{fp}}{d_{fs}}\right)^{1.63}\left(\frac{1}{1 - \varepsilon}\right)^{0.132} \tag{13}$$

In LHTES unit, the progression of the melting process in a PCM is monitored using the melted volume fraction (MVF). This dimensionless measure captures how much of the PCM has melted in comparison to its entire volume. The MVF is computed by evaluating the integral ratio across a specified volumetric domain. A MVF of zero means the PCM is completely solid, while a MVF of one indicates a complete transition to a liquid phase. This tracking is crucial for managing the absorption and release of thermal energy during the PCM's phase transitions.

$$MVF = \frac{\oint_V(\varepsilon\varphi)dV}{\oint_V(\varepsilon)dV} \tag{14}$$

Energy storage capacity is quantified by the rate at which energy accumulates in a system, defined as the total energy stored (Q_{store}) divided by the duration of storage. Q_{store}, the cumulative amount of energy held

Table 1
Properties of copper foam and paffin.

Materials	C_p (J/kg. K)	ρ (kg/ m^3)	k (W/m. K)	μ (Pa.s)	T_{fu} (K)	*Fusion Enthalpy* (J/kg)
Paraffin (solid/ liquid) [40–42,44]	2700/ 2900	916/ 790	0.21/ 0.12	0.0036	324.65	176,000
Copper foam [45]	386	8900	380	–	–	–

within the unit, encompasses both sensible ($Q_{sensible}$) and latent (Q_{latent}) heat contribution.

$$\text{Power} = Q_{\text{store}}/time \tag{15a}$$

$$Q_{\text{store}} = Q_{\text{sensible}} + Q_{\text{latent}} \tag{15b}$$

Equation (16a) details the calculation of energy retention, encompassing both the solid and liquid phases of the PCM, as well as contribution from the heat transfer fluid and the unit's walls. Further, equation (16b) addresses the computation of the total latent heat accumulated in the PCM during its phase transitions from solid to liquid or the reverse.

$$Q_{sensible} = (T - T_0)(\rho C_P)_{MF}\oint_V (1-\varepsilon)dV + \oint_V \left(\int_{T_0}^{T} \varepsilon(\rho C_P)_{PCM}(T)dT\right)dV + (T - T_0)(\rho C_P)_{\text{Wall}}V_{\text{Wall}} + (T - T_0)(\rho C_P)_{\text{HTF}}V_{\text{HTF}} \tag{16a}$$

$$Q_{latent} = \varepsilon\oint_V (\rho_{PCM}\varphi L_{PCM})dV \tag{16b}$$

The thermophysical properties of metal foam and PCM are reported in Table 1.

4. Solution approach and verification

4.1. Numerical method

The governing equations, initial conditions, and boundary constraints were resolved through the application of the Finite Element Method (FEM). To facilitate numerical integration, a weak formulation of the principal equations was derived, enabling the use of Gauss quadrature rules at the elemental level. This process generated a system of algebraic residual equations. For iterative resolution, a damped Newton-Raphson approach with a damping coefficient of 0.9 was implemented to enhance solution convergence [46,47]. Parallel computational efficiency was optimized via the PARDISO solver, which distributed calculations across multiple processing units [48,49]. A relative error tolerance threshold of 1×10^{-4} was enforced to ensure numerical accuracy.

Table 2
Computational duration for each *Nm* scenario.

Nm	Required Time
6	8 hrs, 18 min, and 5 s
7	10 hrs, 36 min, and 56 s
8	13 hrs, 16 min, and 8 s
9	17 hrs 40 min, and 13 s
10	21 hrs 31 min, and 9 s
11	25 hrs, 57 min, and 54 s

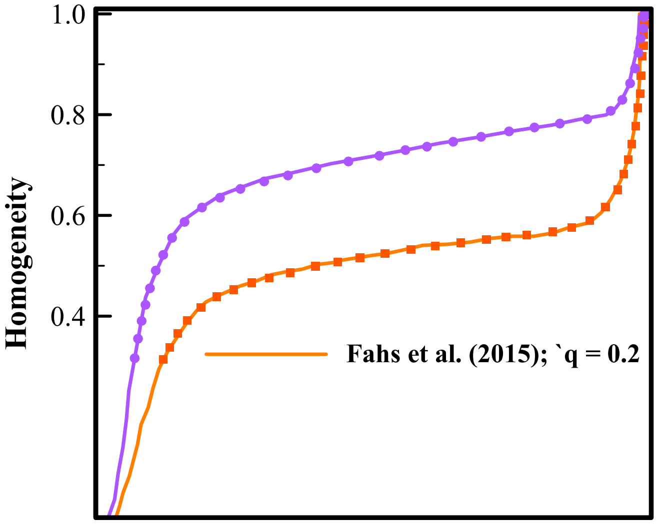

Fig. 4. A comparative analysis of thermal contours between the present simulation results and those reported in [50]. The temperature distributions exhibit close agreement with earlier investigations into natural convection phenomena in anisotropic porous media, validating the consistency of the current computational model. This alignment underscores the accuracy of the methodology for scenarios involving spatially variable permeability and homogeneous thermal conductivity.

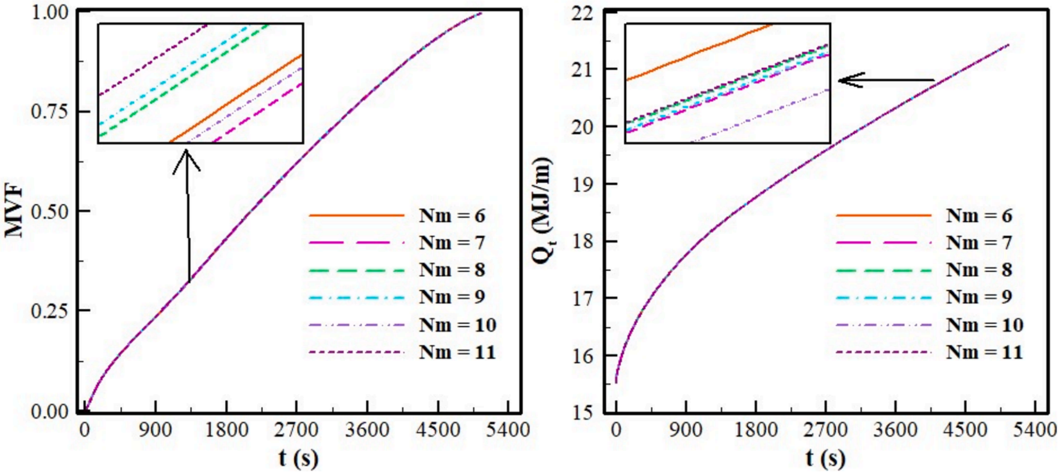

Fig. 3. Grid study: Comparison of MVF and Q_t for *Nm* values of 6, 7, 8, 9, 10, and 11.

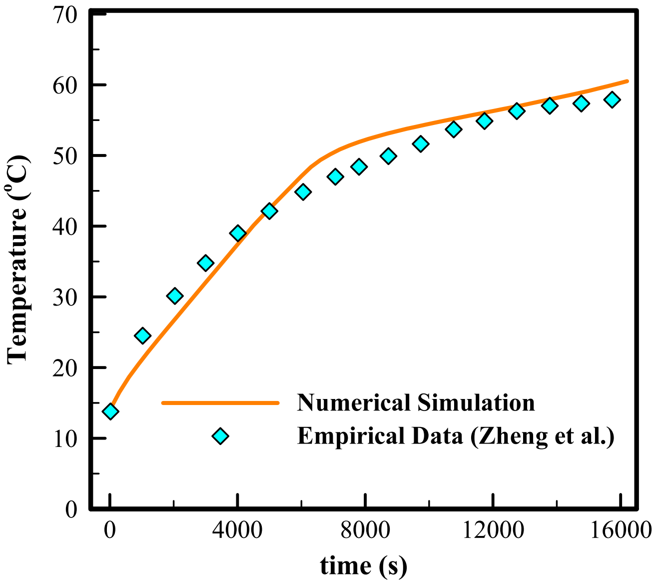

Fig. 5. Comparison with the empirical data from [45] supports the findings of the current study.

4.2. Grid sensitivity evaluation

In evaluating the effects of grid granularity on the numerical simulation precision of phase change processes in an LHTES unit, different grid resolutions were meticulously analyzed. Configurations such as a1, operating under conditions of $Kn = 0.3$ and $\omega = 0^{\circ}$, were specifically assessed to understand the melting dynamics of the PCM. The study utilized an unstructured grid to discretize the computational domain, where the grid density parameter, Nm, controlled the resolution. Detailed insights into this analysis are depicted in Fig. 3, which details each grid design and the corresponding times needed to achieve complete melting and overall heat transfer across grid sizes from Nm = 6 to Nm = 11. Table 2 displays how increasing the resolution from Nm = 6 to Nm = 11 results in increased computational demand, evidenced by longer simulation times, ranging from 8 h and 18 min at the lowest grid density to 25 h and 57 min at the highest. The increasing detail captured by the denser grides not only provides a clearer depiction of the heat transfer processes but also adds sharply to the computational load. For instance, at a grid setting of Nm = 11, the extended duration required for melting calculations indicates the high level of detail involved, whereas the reduced time at Nm = 6 highlights the trade-off between simulation detail and computational efficiency. After thorough testing and evaluation, a grid setting of Nm = 8 was found to offer an effective compromise, balancing the need for accuracy with manageable computational times, totaling 13 h and 16 min. This systemic approach allows for a comprehensive understanding of the effect of grid resolution on the LHTES system's thermal behavior under various operation conditions.

4.3. Validation process for the model

A numerical investigation by Fahs et al. [50] explored heat transfer dynamics and natural convective flow in an anisotropic porous medium exhibiting spatially dependent thermal conductivity. In their analysis, the thermal conductivity gradient was governed by a logarithmic distribution linked to a dimensionless parameter, *Kn*. For consistency in comparative evaluation, the current study retained the definition of *Kn* outlined in [50]. Notably, the earlier work restricted variations in permeability to localized regions while maintaining uniform thermal

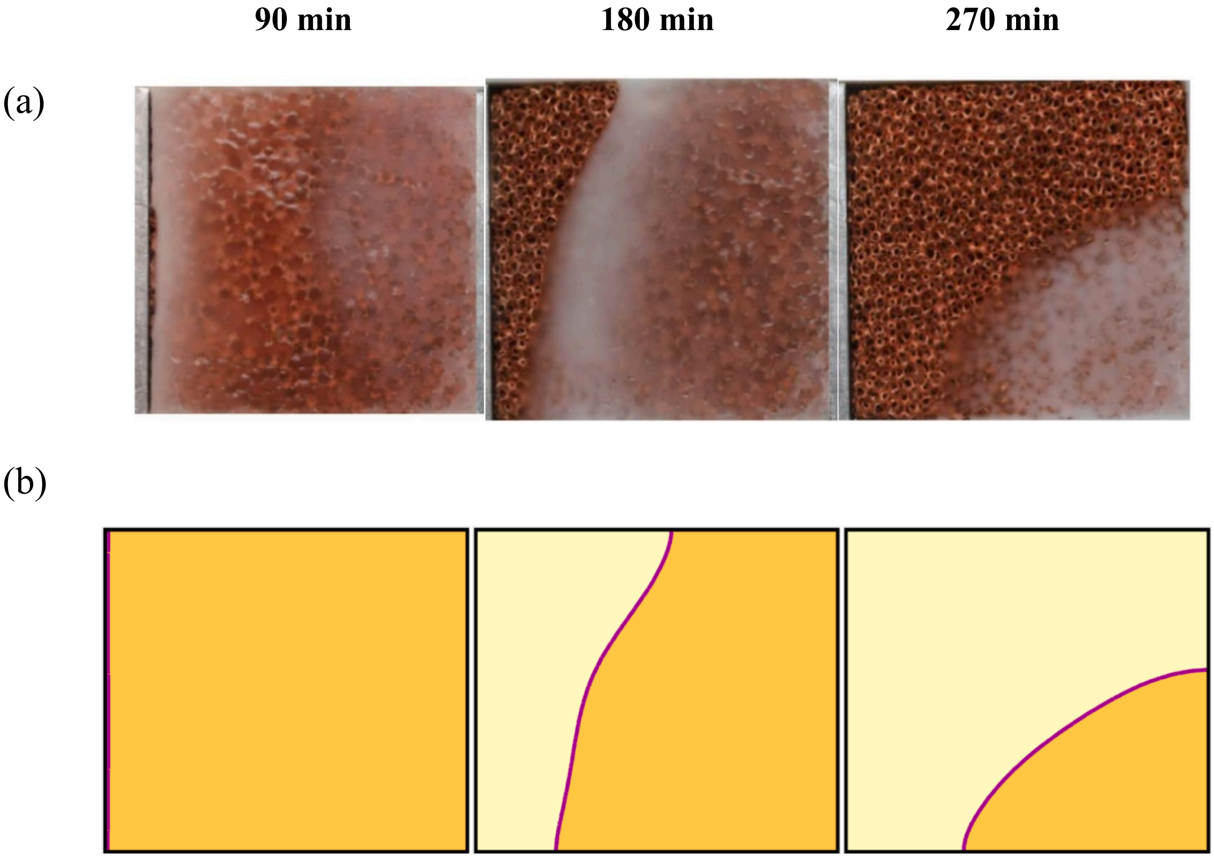

Fig. 6. Melting behavior of the MF composite PCM in an enclosure: (a) experimental data obtained from [45], and (b) results from our recent study.

Table 3
The complete melting time for each configuration.

Cases	Percentage of AMFL occupied	Melting Time (s)		
		80 %	90 %	99.5 %
a1	34.3 %	3678.75	4284.74	5074.18
a2	34.3 %	3674.95	4283.58	5082.20
a3	34.3 %	3733.80	4344.59	5135.15
a4	34.3 %	3731.75	4344.47	5152.80
b1	45.3 %	3616.80	4212.90	4994.57
b2	45.3 %	3602.04	4199.09	4983.63
b3	45.3 %	3722.39	4329.76	5119.30
b4	45.3 %	3709.66	4318.71	5124.98
c1	56.3 %	3563.50	4152.98	4927.90
c2	56.3 %	3536.47	4119.30	4887.54
c3	56.3 %	3707.98	4315.21	5108.43
c4	56.3 %	3685.67	4290.67	5090.04
d1	67.2 %	3520.12	4106.47	4875.38
d2	67.2 %	3484.24	4056.90	4812.90
d3	67.2 %	3679.38	4286.11	5081.30
d4	67.2 %	3656.01	4256.98	5044.88
a0	0 %	3805.02	4433.50	5243.11

conductivity. To validate computational accuracy, dimensionless temperature profiles from the present simulations were benchmarked against those reported in [50] under conditions where $Kn = 2.0$ (Fig. 4). This comparison focused on scenarios involving unidirectional permeability variation (x-axis) with homogeneity preserved along the y-axis. The observed alignment between the two datasets confirms robust consistency with prior findings, underscoring the reliability of the numerical approach.

In the study documented by Zheng et al. [45] the analysis focused on three distinct heating positions- left, bottom, and top- to discover the melting behavior of the copper foam/paraffin composite PCM in a rectangular polyethylene enclosure. It assessed the impact of a constant heat flux of 1150 W applied at a heating rate of 10℃ per minute to the composite's left boundary, while the other walls remained insulated. The experimental setup included a 1005 × 10 × 30 mm electrical heater, and various parameters such as temperature distribution and solid–liquid interface development were recorded. Operating within a temperature range of 20 to 80℃ under a laminar flow regime, the system demonstrated substantial thermal activity. The copper MF's porosity and matrix concentration, at 0.95 and 5 pores per inch respectively, played a key role in affecting the melting dynamics of the paraffin wax. Zheng et al. [45] employed a uniform metal foam structure, where Kn was assumed to be zero. This assumption, representing a uniform metal foam, is also adopted in the present study for comparison purposes. The study also noted that the composite's effective thermal conductivity was improved due to the copper foam's structure, which facilitated quicker heat transfer to the inner parts of the PCM. Fig. 5 shows the mean temperature profile across a longitudinal line positioned 2.5 cm from the heat application plane, comparing experimental data with numerical simulations over time. The outputs showed a strong correlation between the two models, indicating the accuracy of the simulations. Fig. 6 illustrates the phase change from liquid to solid at various stages of the melting process, emphasizing that the simulation results, which include structural details, edge definitions, and thermal gradients, closely align with the experimental findings. The agreement between empirical data and numerical modeling in this figure further validates the simulation's reliability.

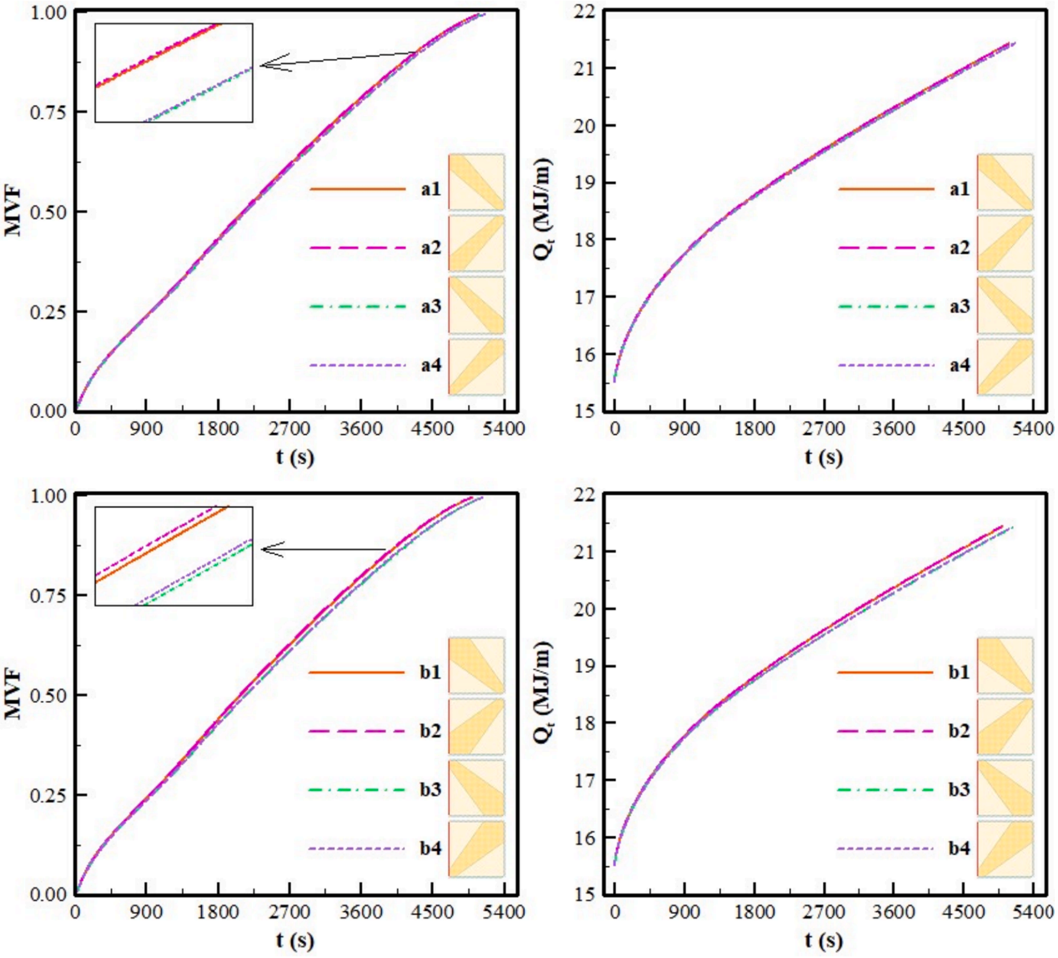

Fig. 7. MVF, total heat transfer (Q_t) over the melting progression for different configurations.

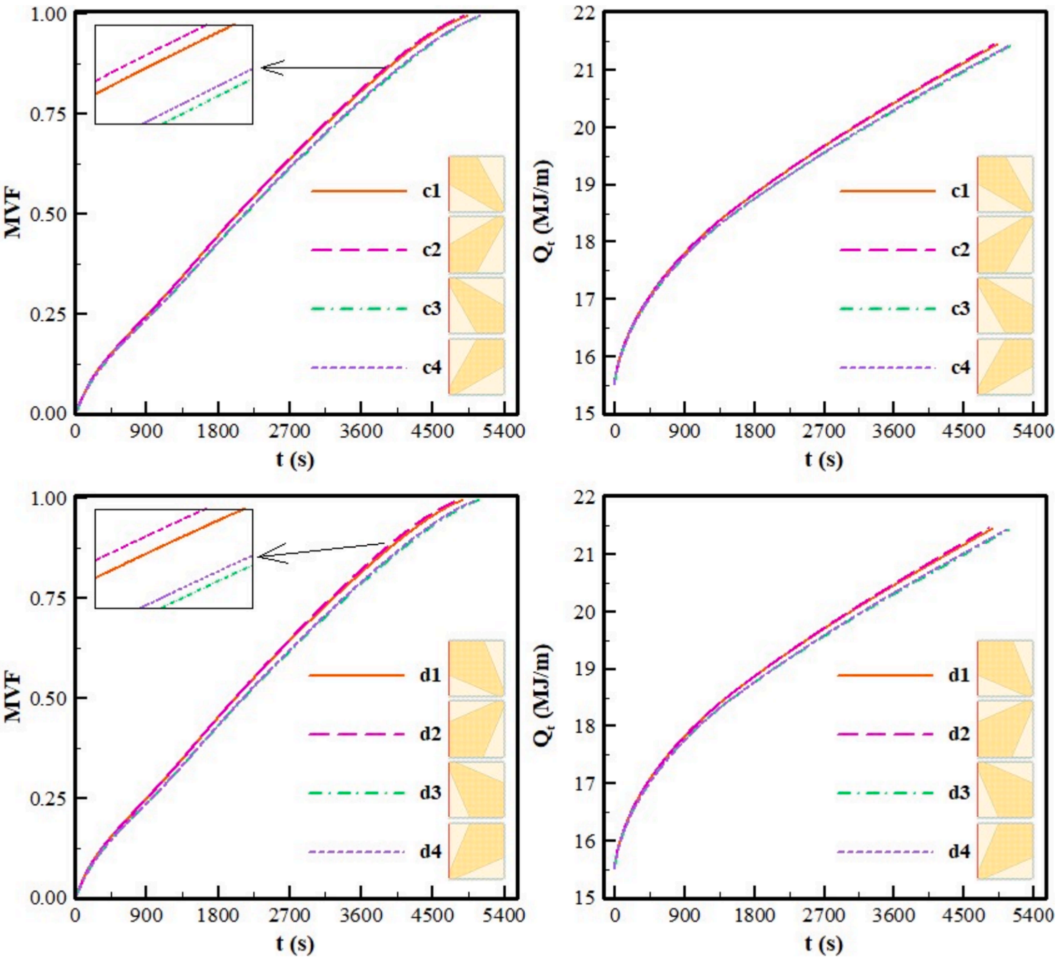

Fig. 7. (*continued*).

5. Results and discussion

The effect of the AMFL size and its orientation on the melting behavior and energy stored is first addressed. Graphs of isotherms and melting contours are then plotted to better illustrate their variations with the various AMFL configurations.

Table 3 summarizes the total melting times for all the considered configurations of the AMFL. First, it is seen that for a given AMFL orientation (1 to 4), increasing the AMFL size and its percentage in the total MF in the cavity (cases a to d) leads to lower PCM melting times, which is an indicator of the fact that the presence of the anisotropic porous foam can effectively help in accelerating the PCM melting. Moreover, in each case (a to d), it is found that the melting time in configurations 1 and 2 is lower that the configurations 3 and 4. By looking at the geometries, this indicates that orienting the AMFL in a way that its larger part is near the hot wall accelerates PCM melting compared to the orientations where the larger part of the cavity is placed near the right wall. This further illustrates that not only adding an AMFL in the cavity affects the PCM melting, but also the orientation at which the AMFL is placed.

The variations of the melted volume fraction MVF and the total energy stored Qt as functions of time are depicted in Fig. 7. The shapes of variations are overall the same in all the considered configurations. The MVF is initially zero, then starts gradually increasing as melting occurs until finally reaching one once the whole PCM has melted. It is observed that the curves for the different orientations are very close to each other, mainly for low AMFL size. For instance, the curves a1 to a4 almost coincide. Here, the AMFL encompasses 34.3 % of the total MF area. When this percentage is increased, the change of the MVF curves with the AMFL orientation becomes more apparent. This indicates that the impact of the AMFL orientation is only apparent when the size of AMFL is large enough to alter the PCM melting behavior. As for Qt, its variation follows that of the MVF. Initially, Qt increases with a strong slope, as the temperature gradient at the melting interface is at its highest. Then, as the PCM melts and the volume of liquid PCM increases, Qt keeps rising but at a more gradual slope. Also similar to the MVF, Qt is higher when the AMFL is places with its larger side near the hot wall compared to the opposite orientation.

To provide quantitative comparison, the reduction percentages in the total melting time for various configurations with respect to the least efficient one are plotted in Fig. 8 for the different AMFL sizes considered. To better compare the results, the total melting time for a unit completely filled just with just uniform metal foam (a0). This case is used as a baseline and is highlighted as a0 in the bar chart. The total melting time for the uniform MF is 5243.11 s, showing that melting takes significantly longer compared to the cases where AMFL is integrated. In all cases (a to d), the configurations 3 and 4 lead to the longest melting time. The difference between these two configurations does not exceed 0.72 % for all the cases, indicating that placing the large side of the AMFL to the right leads to similar results and slows down melting, whether it is at the top or bottom right corner. On the other hand, placing this large side to the left, near the hot wall, can strongly reduce the melting time, mainly when the percentage of the AMFL in the cavity is high. For instance, in the case (b) where the AMFL covers 45.3 % of the total MF, orienting the AMFL in a way that its larger side is at the bottom left corner (b2) reduces the melting time by 2.76 % compared to the case

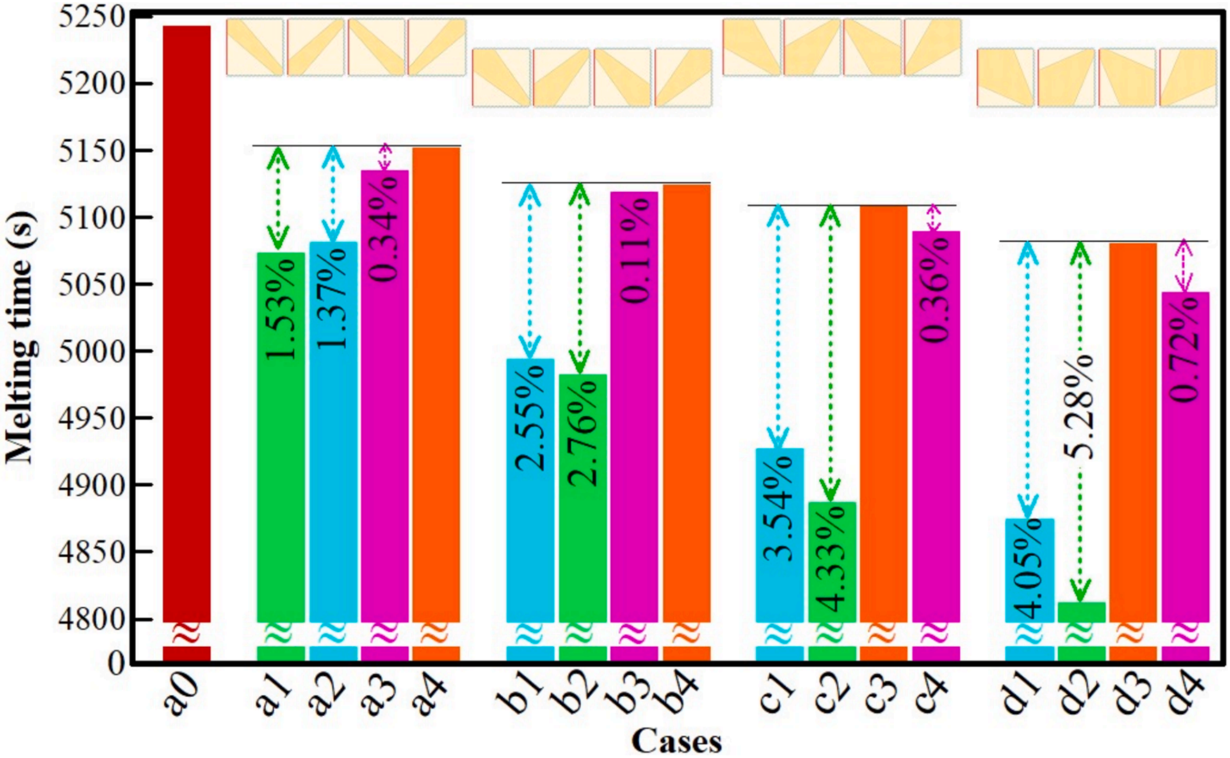

Fig. 8. The total melting times across different configurations and also the uniform MF case (a0). Each Column's percentage indicates the decrease in melting time relative to the least efficient configuration at corresponding scales, highlighted in red, with the most efficient designs marked in green. (For interpretation of the references to colour in this figure legend, the reader is referred to the web version of this article.)

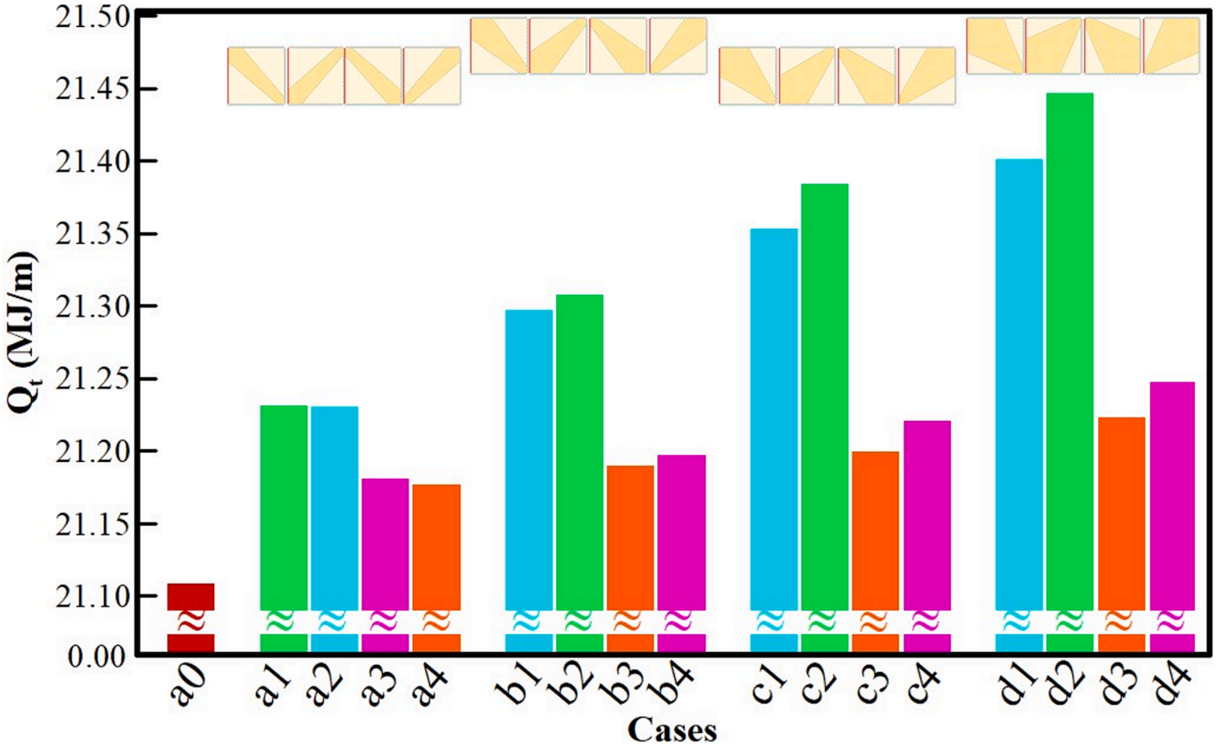

Fig. 9. The total energy stored at t = 80 min for different configurations including the uniform MF case (a0). Columns in red in each scale represent the least efficient designs, while those in green indicate the most efficient. (For interpretation of the references to colour in this figure legend, the reader is referred to the web version of this article.)

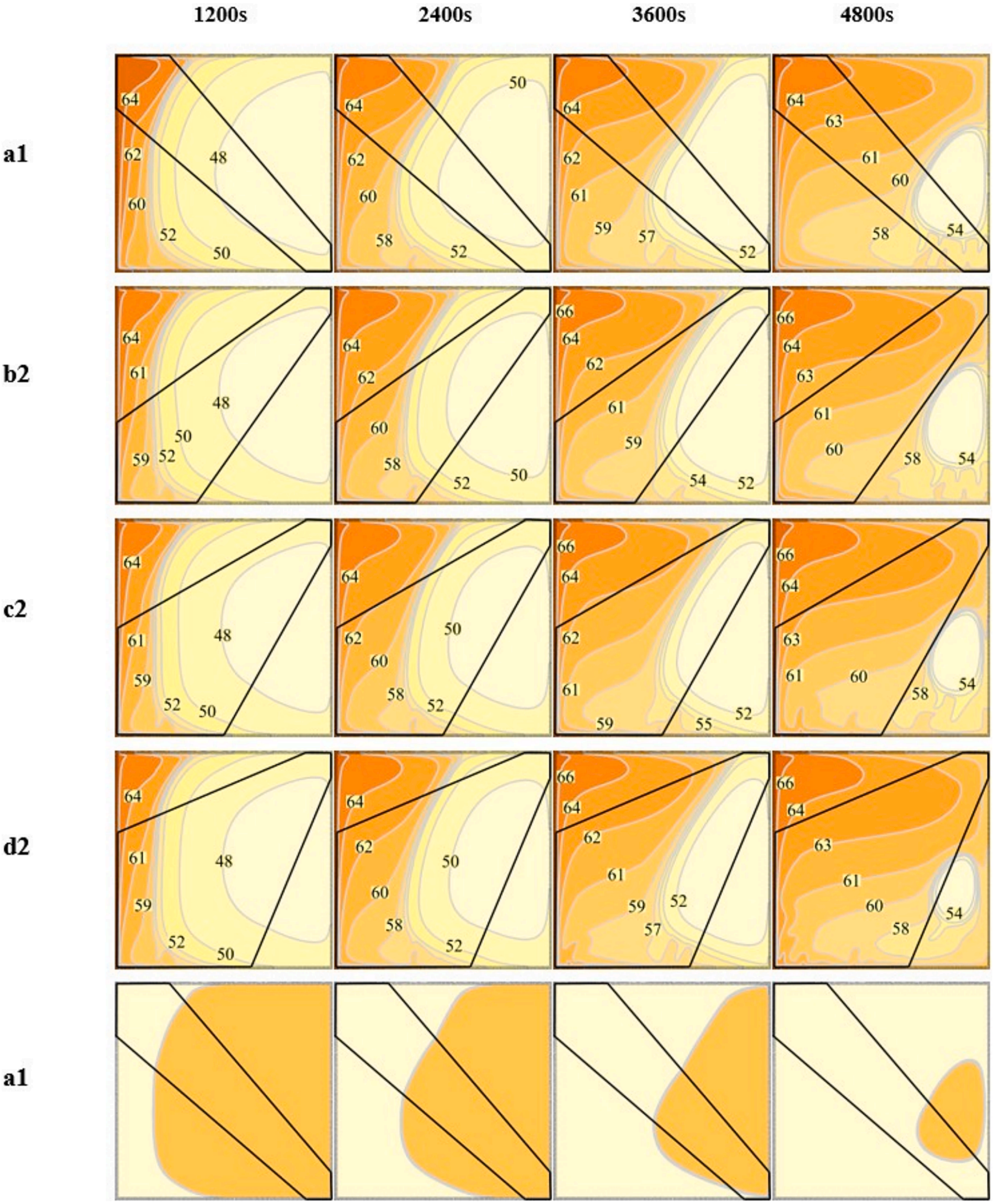

Fig. 10. Isotherms in Celsius degree and MVF contours for the most efficient configuration of each scale.

where it is at the bottom right (b3). When the AMFL encompasses 67.2 % of the total area (case d), up to 5.28 % decrease in the melting time can be obtained for the aforementioned change in the orientation of the AMFL. This confirms the fact that both the size and orientation of the AMFL can affect the PCM melting behavior in the enclosure. Nonetheless, it can be also seen from the figure that the orientation of the AMFL role is more important than its size. For instance, comparing the cases d3 and c2 shows that the melting time is 4.1 % faster in the latter even though the percentage of AMFL in the former is higher. This is because the larger side of the anisotropic layer is placed near the hot wall in the c2, while it is near the cold one in d3. This result illustrates that the orientation of the AMFL is as important as its size, and that increasing the size of the AMFL is not enough to optimize the PCM melting, but the layer should be placed in the good direction.

The shortest melting time with AMFL occurs in case d2, at 4812.90 s, while the reference case without AMFL—despite having the same uniform porosity and metal foam amount—has a melting time of 5243.11 s. Thus, AMFL has reduced the melting time by 8.2 % for case d2 compared

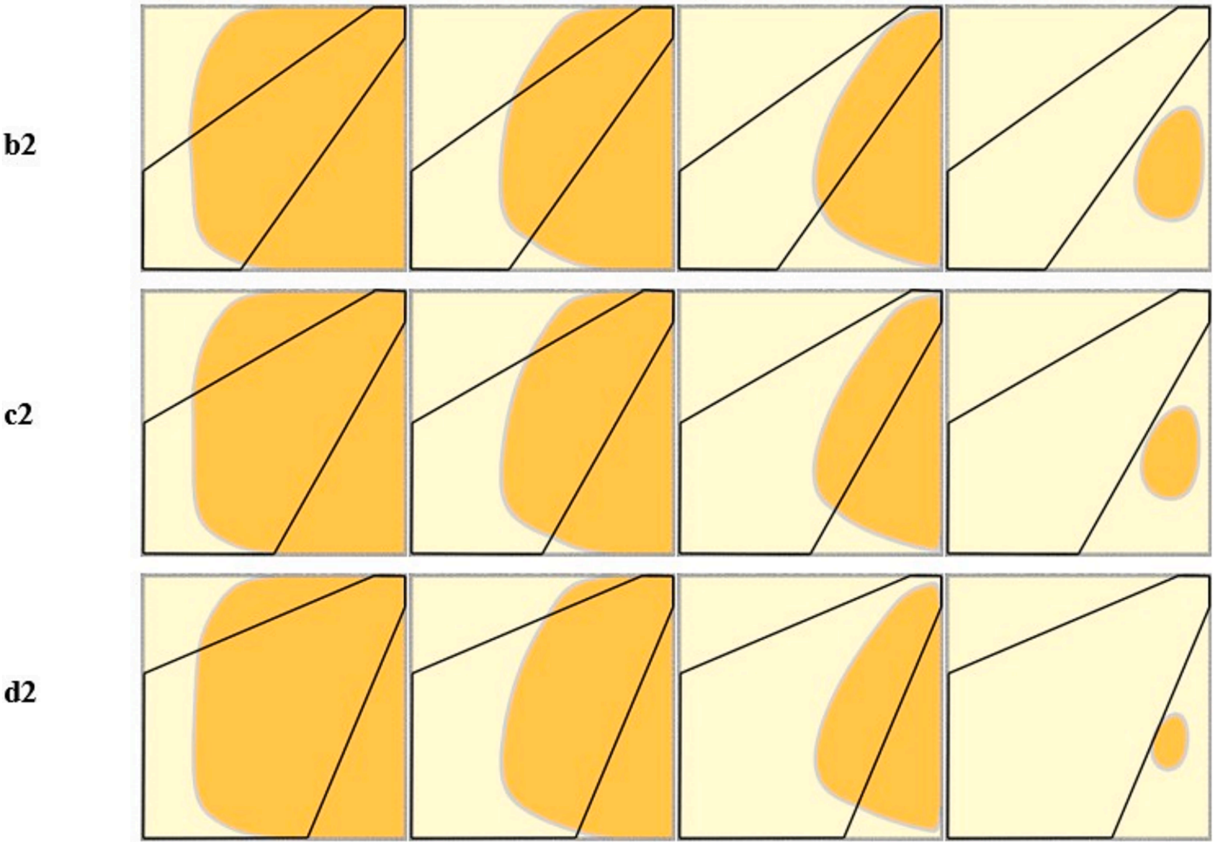

Fig. 10. (*continued*).

to the reference case a0.

Fig. 9 shows the values of Qt with the different AMFL configurations, with indications to the least (red columns) and most (green columns) efficient ones for each AMFL size. For the a0 case, where the uniform MF is used as a baseline, Qt reaches only 21.11 MJ/m after 80 min of melting, greatly lower than the cases integrated with AMFL. Naturally, the configurations experiencing the shortest melting time are the ones providing the highest Qt. Among the various configurations, the most amount of stored energy is obtained for the AMFL with the highest area percentage and having its large side at the bottom left corner. Conversely, Qt is minimum when the AMFL is small in size and is oriented in the opposite direction.

The isothermal patterns and the MVF contours are plotted in Fig. 10 for selected AMFL configurations covering the different sizes considered. There are observations that are common to the various cases. Initially, the PCM starts melting near the hot wall, where the temperature is higher than its melting temperature. The heat transfer is dominated by conduction, as indicate the almost vertical isothermal lines. As time passes, the zone of melted PCM starts to increase and the isotherms are disturbed, indicating a shift from conduction to convective heat transfer. The hot PCM near the left goes upwards and gets replaced by colder PCM moving downwards. Near the top, the melted PCM exchanges heat with the solid PCM, melts it and gets cooled as it moves down the melting interface, leading to more melting in the upper half of the cavity compared to its lower one. After sufficiently long time, after most of the PCM has melted, the isotherms at the cavity center become quasi horizontal, which indicates that convection has overtaken the heat transfer in the liquid PCM. This behavior can illustrate the changes in PCM melting with the AMFL configurations. As can be seen, the size of the remaining solid PCM becomes smaller when the AMFL percentage in the cavity is raised. In other words, using a larger anisotropic layer accelerates PCM melting. Indeed, in this layer, the conductivity and permeability of the medium are increased along the flow direction, which enhances the convective effects in the PCM and consequently augments its melting rate. On a broader level, this observation indicates that it is indeed possible to improve the PCM melting and energy storage by simply changing the porous foam structure through anisotropic model, without having to change the porosity by altering the amount of metal used and the resulting energy storage capacity.

6. Conclusions

The advantage of replacing conventional metal foams by anisotropic ones with the purpose of improving PCM melting and energy storage was investigated numerically. To do so, a PCM-filled porous square cavity heated on its left side was considered. The other walls were kept adiabatic. An asymmetric hexagonal shaped anisotropic metal foam layer (AMFL) was placed inside the original isotropic metal foam (MF). The size and orientation of the AMFL layer were varied. In particular, four sizes were considered by changing the percentage of MF that the AMFL covers in the cavity (34.3 %, 45.3 %, 56.3 %, and 67.2 %). The orientation of the AMFL was varied by changing the location at which its larger side was placed, at the four corners of the enclosure. The equations governing the flow and thermal behaviors of the PCM were presented and solved by employing the finite element method. Results in the form of graphs of the melted fraction of the PCM and the energy stored, as well as contours of isotherms and melting interface were plotted. The outcomes that it is indeed possible to improve the PCM performance by adding the AMFL layer. The importance of this result lies in the fact that using an anisotropic foam means a change in the structure of the foam, without affecting its porosity and the amount of the metallic matrix and, most importantly, the energy density in the cavity. The impact of the AMFL on enhancing the PCM melting was obtained to be more important when the size of the layer was increased.

In addition, the orientation of the layer was also found to be essential in controlling the PCM melting. Locating the large side of the AMFL near the hot wall has a higher contribution to PCM melting compared to the opposite direction. Up to 5.28 % reduction in the melting duration was obtained for such a change in the AMFL orientation. This is related to the direction of the permeability in the foam, which helps in improving the convective flow of the melted PCM. This flow initiates near the hot wall and it intensifies when the AMFL is placed in that location. AMFL reduced the melting time by 8.2 % in case d2 to 4812.90 s compared to the reference case's 5243.11 s.

The scalability of LHTES can be achieved by connecting multiple units in series for high temperature differentials or in parallel to increase the volume flow rate of HTF. While using heterogeneous metal foams may raise manufacturing costs if traditional production and assembly methods are applied, AMFL could reduce these costs in printing methods. This is because AMFL designs can be printed as part of a uniform structure, minimizing the need for complex assembly. The present study provides an overview of the effectiveness of AMFL layers in enhancing LHTES performance from thermal perspective. Given the potential of AMFL to accelerate energy storage processes, future research should focus on the printing or manufacturing of these designs, accompanied by experimental validation and thermal energy storage performance tests.

CRediT authorship contribution statement

Masoud Mozaffari: Writing – original draft, Visualization, Validation, Software, Methodology, Formal analysis, Data curation, Conceptualization. **Ahmad Hajjar:** Writing – review & editing, Writing – original draft, Methodology, Investigation, Formal analysis. **Mikhail Sheremet:** Writing – review & editing, Project administration, Methodology, Investigation, Formal analysis. **Obai Younis:** Writing – review & editing, Writing – original draft, Resources, Investigation, Data curation, Conceptualization. **Mohammad Ghalambaz:** Writing – review & editing, Writing – original draft, Supervision, Methodology, Conceptualization.

Declaration of competing interest

The authors declare that they have no known competing financial interests or personal relationships that could have appeared to influence the work reported in this paper.

Acknowledgements

This study is supported via funding from Prince Sattam bin Abdulaziz University project number (PSAU/2023/R/1444). This research of Mikhail Sheremet and Mohammad Ghalambaz was supported by the Tomsk State University Development Programme (Priority-2030).

Data availability

Data will be made available on request.

References

[1] K. Shank, S. Tiari, A review on active heat transfer enhancement techniques within latent heat thermal energy storage systems, Energies 16 (10) (2023) 4165.
[2] M. Thonon, G. Fraisse, L. Zalewski, M. Pailha, Simultaneous charging and discharging processes in latent heat thermal energy storage: A review, Thermal Science and Engineering Progress, (2023) 102299.
[3] Z.H. Low, Z. Qin, F. Duan, A review of fin application for latent heat thermal energy storage enhancement, J. Storage Mater. 85 (2024) 111157.
[4] N. Najafpour, O. Adibi, Melting enhancement of latent heat thermal energy storage by implementing new geometric design, Appl. Therm. Eng. 239 (2024) 122066.
[5] M.T. Alam, V. Garg, V. Soni, A.K. Gupta, Effect of enclosure design with composite/nano-enhanced/dual phase change material on melting response of latent heat storage systems, Chem. Eng. Res. Des. 214 (2025) 125–143.
[6] K. Sudarmozhi, D. Iranian, N. Alessa, Investigation of melting heat effect on fluid flow with brownian motion/thermophoresis effects in the occurrence of energy on a stretching sheet, Alex. Eng. J. 94 (2024) 366–376.
[7] H. Togun, H.S. Sultan, H.I. Mohammed, A.M. Sadeq, N. Biswas, H.A. Hasan, R. Z. Homod, A.H. Abdulkadhim, Z.M. Yaseen, P. Talebizadehsardari, A critical review on phase change materials (PCM) based heat exchanger: different hybrid techniques for the enhancement, J. Storage Mater. 79 (2024) 109840.
[8] K. Sudarmozhi, D. Iranian, Q.M. Al-Mdallal, Revolutionizing energy flow: Unleashing the influence of MHD in the presence of free convective heat transfer with radiation, International Journal of Thermofluids 22 (2024) 100662.
[9] S. Karthik, D. Iranian, H. Alhazmi, I. Khan, A. Singh, Heat transfer due to electromagnetic radiation of MHD Powell-Eyring fluid with mass diffusion via Lie symmetry scaling, Case Stud. Therm. Eng. 58 (2024) 104348.
[10] S.M. Mousavi, F. Khanmohammadi, A.A.R. Darzi, Magnetic influence on phase change materials for optimized thermal energy storage: a comprehensive review and prospective insights, J. Storage Mater. 89 (2024) 111625.
[11] N. Modi, X. Wang, M. Negnevitsky, Solar hot water systems using latent heat thermal energy storage: perspectives and challenges, Energies 16 (4) (2023) 1969.
[12] A. Kumar, A. Kumar, Heat transfer analysis in thermal energy storage—a comprehensive review-based latent heat storage system, Energy Storage 5 (6) (2023) e434.
[13] W. Ye, D. Jamshideasli, J.M. Khodadadi, Improved performance of latent heat energy storage systems in response to utilization of high thermal conductivity fins, Energies 16 (3) (2023) 1277.
[14] B. Buonomo, M.R. Golia, O. Manca, S. Nardini, A review on thermal energy storage with phase change materials enhanced by metal foams, Therm. Sci. Eng. Prog. (2024) 102732.
[15] A. Andreozzi, P. Asinari, A. Barletta, V. Bianco, J.A. Bocanegra, P.V. Brandão, B. Buonomo, R. Cappabianca, M. Celli, E. Chiavazzo, Heat transfer and thermal energy storage enhancement by foams and nanoparticles, Energies 16 (21) (2023) 7421.
[16] V.V. Upadhyay, S. Singhal, A review of current developments in the use of materials with latent heat phase changes for the storage of thermal energy, Mater. Today Proc. (2023).
[17] J. Shi, H. Du, Z. Chen, S. Lei, Review of phase change heat transfer enhancement by metal foam, Appl. Therm. Eng. 219 (2023) 119427.
[18] Z. Li, X. Wang, Y. Li, J. Guo, X. Huang, X. Yang, Y.-L. He, Design and evaluation of metal foam horizontal tube-and-shell phase change accumulator: optimal position distribution of heating tubes, Int. J. Heat Fluid Flow 107 (2024) 109367.
[19] Z. Haddad, F. Iachachene, M.A. Sheremet, E. Abu-Nada, Numerical investigation and optimization of melting performance for thermal energy storage system partially filled with metal foam layer: new design configurations, Appl. Therm. Eng. 223 (2023) 119809.
[20] N.S. Bondareva, M.A. Sheremet, Numerical simulation of heat transfer performance in an enclosure filled with a metal foam and nano-enhanced phase change material, Energy 296 (2024) 131123.
[21] W.Q. Li, T.Y. Zhang, B.B. Li, Z.R. Xue, H. Wang, D. Zhang, Enhanced energy management performances of passive cooling, heat storage and thermoelectric generator by using phase change material saturated in metal foam, Int. J. Therm. Sci. 184 (2023) 107869.
[22] Y. Li, Z. Niu, X. Gao, J. Guo, X. Yang, Y.-L. He, Effect of filling height of metal foam on improving energy storage for a thermal storage tank, Appl. Therm. Eng. 229 (2023) 120584.
[23] R. Hu, X. Huang, X. Gao, L. Lu, X. Yang, B. Sundén, Design and assessment on a bottom-cut shape for latent heat storage tank filled with metal foam, Int. J. Therm. Sci. 197 (2024) 108757.
[24] M. Ghalambaz, M. Fteiti, O. Younis, M. Sheremet, H.A. Hasan, An improved latent heat thermal energy storage using two layers of metal foams, Appl. Therm. Eng. 234 (2023) 121319.
[25] J. Lei, Y. Huang, C. Yang, X. Xu, Z. Li, Y. Zhang, Numerical study on heat transfer enhancement of shell-and-tube thermal energy storage unit using metal foams with non-uniform porosity, Int. J. Green Energy 20 (10) (2023) 1026–1039.
[26] J. Kong, H. Zuo, K. Zeng, Y. Lu, H. Xu, X. Zhang, H. Yang, H. Chen, Investigation of optimization methods for metal foam with two-dimensional porosity gradient in shell-and-tube latent heat storage, J. Storage Mater. 63 (2023) 107004.
[27] T. Si, W. Cui, T. Ma, L. Lu, Q. Wang, Numerical investigation on thermal performance of phase change materials embedded in functionally graded metal foam, J. Storage Mater. 81 (2024) 110482.
[28] P. Du, M. Wang, X. Zhong, B. Chen, Z. Li, R. Zhou, Y. Huo, Z. Rao, Anisotropic porous skeleton for efficient thermal energy storage and enhanced heat transfer: experiments and numerical models, J. Storage Mater. 56 (2022) 106021.
[29] M. Ghalambaz, M. Aljaghtham, A.J. Chamkha, A. Abdullah, A. Alshehri, M. Ghalambaz, Anisotropic metal foam design for improved latent heat thermal energy storage in a tilted enclosure, Int. J. Mech. Sci. 238 (2023) 107830.
[30] M. Ghalambaz, M. Aljaghtham, A.J. Chamkha, A. Abdullah, I. Mansir, M. Ghalambaz, Mathematical modeling of heterogeneous metal foams for phase-change heat transfer enhancement of latent heat thermal energy storage units, App. Math. Model. 115 (2023) 398–413.
[31] H.S. Sultan, M.H. Ali, J. Shafi, M. Fteiti, M. Baro, F. Alresheedi, M.S. Islam, T. Yusaf, M. Ghalambaz, Improving phase change heat transfer in an enclosure filled by uniform and heterogenous metal foam layers: a neural network design approach, J. Storage Mater. 85 (2024) 110954.
[32] P. Guo, C. Zhao, W. Xu, N. Sheng, Z. Rao, C. Zhu, Ice templated honeycomb-like porous copper foam to improve the anisotropic thermal transfer property of phase change composites, J. Alloy. Compd. 991 (2024) 174536.

[33] Q. Ren, Z. Wang, T. Lai, J.F. Zhang, Z.G. Qu, Conjugate heat transfer in anisotropic woven metal fiber-phase change material composite, Appl. Therm. Eng. 189 (2021) 116618.
[34] S. Zhang, Y. Yao, Y. Jin, Z. Shang, Y. Yan, Heat transfer characteristics of ceramic foam/molten salt composite phase change material (CPCM) for medium-temperature thermal energy storage, Int. J. Heat Mass Transf. 196 (2022) 123262.
[35] M. Ghalambaz, A.A. Melaibari, A.J. Chamkha, O. Younis, M. Sheremet, Phase change heat transfer and energy storage in a wavy-tube thermal storage unit filled with a nano-enhanced phase change material and metal foams, J. Storage Mater. 54 (2022) 105277.
[36] D.A. Nield, A. Bejan, Convection in porous media, Springer, 2006.
[37] Y. Yao, H. Wu, Interfacial heat transfer in metal foam porous media (MFPM) under steady thermal conduction condition and extension of Lemlich foam conductivity theory, Int. J. Heat Mass Transf. 169 (2021) 120974.
[38] C. Zhao, J. Wang, Y. Sun, S. He, K. Hooman, Fin design optimization to enhance PCM melting rate inside a rectangular enclosure, Appl. Energy 321 (2022) 119368.
[39] M. Ghalambaz, M. Aljaghtham, A.J. Chamkha, A. Abdullah, A. Alshehri, M. Ghalambaz, An anisotropic metal foam design for improved latent heat thermal energy storage in a tilted enclosure, Int. J. Mech. Sci. (2022) 107830.
[40] A.I.N. Korti, H. Guellil, Experimental study of the effect of inclination angle on the paraffin melting process in a square cavity, J. Storage Mater. 32 (2020) 101726.
[41] A. Agarwal, R. Sarviya, Characterization of commercial grade paraffin wax as latent heat storage material for solar dryers, Mater. Today Proc. 4 (2) (2017) 779–789.
[42] N. Ukrainczyk, S. Kurajica, J. Šipušić, Thermophysical comparison of five commercial paraffin waxes as latent heat storage materials, Chem. Biochem. Eng. Q. 24 (2) (2010) 129–137.
[43] Y. Yao, H. Wu, Macroscale modeling of solid–liquid phase change in metal foam/paraffin composite: effects of paraffin density treatment, thermal dispersion, and interstitial heat transfer, J. Therm. Sci. Eng. Appl. 13 (4) (2021).
[44] N.B. Khedher, M. Sheremet, A.M. Hussin, S.A.M. Mehryan, M. Ghalambaz, The effect of hot wall configuration on melting flow of nano-enhanced phase change material inside a tilted square capsule, J. Storage Mater. 69 (2023) 107921.
[45] H. Zheng, C. Wang, Q. Liu, Z. Tian, X. Fan, Thermal performance of copper foam/paraffin composite phase change material, Energ. Conver. Manage. 157 (2018) 372–381.
[46] C.T. Kelley, in: Solving Nonlinear Equations with Newton's Method, SIAM, pp. 1-25.
[47] P. Deuflhard, Newton Methods for Nonlinear Problems: Affine Invariance and Adaptive Algorithms, Springer Publishing Company, Incorporated, 2011.
[48] M. Bollhöfer, O. Schenk, R. Janalík, S. Hamm, K.K. Gullapalli, State-of-The-Art Sparse Direct Solvers, ArXiv, abs/1907.05309 (2019).
[49] M. Bollhöfer, A. Eftekhari, S. Scheidegger, O. Schenk, Large-scale sparse inverse covariance matrix estimation, SIAM J. Sci. Comput. 41 (1) (2019) A380–A401.
[50] M. Fahs, A. Younes, A. Makradi, A reference benchmark solution for free convection in a square cavity filled with a heterogeneous porous medium, Numer. Heat Transf. B Fundam. 67 (5) (2015) 437–462.